Tapish Agarwal
Technion-Israel Institute of Technology,
Technion City,
Haifa 32000, Israel

Iman Rahbari
Zucrow Laboratories,
Purdue University,
West Lafayette, IN 47907

Jorge Saavedra
Zucrow Laboratories,
Purdue University,
West Lafayette, IN 47907

Guillermo Paniagua
Zucrow Laboratories,
Purdue University,
West Lafayette, IN 47907

Beni Cukurel
Technion-Israel Institute of Technology,
Technion City,
Haifa 32000, Israel
e-mail: beni@cukurel.org

Multifidelity Analysis of Acoustic Streaming in Forced Convection Heat Transfer

This research effort is related to the detailed analysis of the temporal evolution of thermal boundary layer(s) under periodic excitations. In the presence of oscillations, the nonlinear interaction leads to the formation of secondary flows, commonly known as acoustic streaming. However, the small spatial scales and the inherent unsteady nature of streaming have presented challenges for prior numerical investigations. In order to address this void in numerical framework, the development of a three-tier numerical approach is presented. As a first layer of fidelity, a laminar model is developed for fluctuations and streaming flow calculations in laminar flows subjected to traveling wave disturbances. At the next level of fidelity, two-dimensional (2D) U-RANS simulations are conducted across both laminar and turbulent flow regimes. This is geared toward extending the parameter space obtained from laminar model to turbulent flow conditions. As the third level of fidelity, temporally and spatially resolved direct numerical simulation (DNS) simulations are conducted to simulate the application relevant compressible flow environment. The exemplary findings indicate that in certain parameter space, both enhancement and reduction in heat transfer can be obtained through acoustic streaming. Moreover, the extent of heat transfer modulations is greater than alterations in wall shear, thereby surpassing Reynolds analogy. [DOI: 10.1115/1.4045306]

Keywords: acoustic streaming, Stokes layer, forced convection heat transfer, heat transfer enhancement, heat transfer reduction

1 Introduction

The major portion of literature on heat transfer enhancement either deals with the addition of turbulence to the flow inside a heat exchanger or the control of boundary layer separation and reattachment. To this end, many active and passive methods have been used [1]; typical examples include mixing of particles in the heat carrier, flow suction, jets, surface vibration, installation of ribs, roughening of surfaces, or the use of flow swirlers. The most efficient heat-transfer enhancement method should alter the flow only near the wall, which limits the overall pressure loss while promoting locally large temperature gradients.

The periodic perturbation of boundary layers can be used to alter the near wall flow without significantly affecting the mainstream. The fundamental physical principle of periodically perturbed boundary layers can be explained by the aerodynamic Galilean transformed version of Second Stokes problem. For negligible convective terms, the physics reduces to the one-dimensional parabolic diffusion equation. Assuming a harmonic oscillation for the freestream component, the viscous boundary layer response expresses shear to originate from the wall and to propagate into the fluid by means of an exponentially damped wave of varying phase lag. The length scale associated with this attenuation process determines the thin near wall region which contains the viscous effects and is known as the Stokes layer (η_s). Due to the nonlinearity of the convective acceleration terms, a nonzero mean flow is generated from zero-mean fluctuations, known as "steady streaming." Thereby, an ordered formation of periodic vortex pairs arises parallel to the wall, inside and outside of the Stokes layer.

In the case of nonvanishing mean flows (advection), there is an interaction between the Stokes and steady boundary layers. This leads to the formation of a secondary layer within which the effect of fluctuations is significant. The layer thickness depends on the fluctuation amplitude, the frequency, and the viscosity. At the high frequency oscillation limit, this secondary layer is significantly thinner than the steady aerodynamic boundary layer, which enables its independent treatment [2–4]. In contrast, for lower frequency oscillations, their interaction is coupled, streaming induces additional gradients near the wall.

Traditionally, the streaming problem has been attempted to be solved using reduced order modeling. For a flat plate laminar boundary layer, a semi-analytical approach to calculate streaming velocity for standing wave type disturbances has been proposed by Lin [5]. However, it has never been applied to actual computations of streaming velocities. This is likely due to its applicability limitations to high frequency and standing wave type disturbances. Under the high frequency approximation, the theoretical framework involves a separate solution for the fluctuating component of the flow, which can be used to calculate the nonlinear fluctuating flow contribution to the mean flow.

An alternative method, which employs linearization of small oscillation amplitudes is proposed by Lighthill. The assumption that the amplitudes of temporal oscillations is small allows for the problem to be solved by first invoking the mean flow equation, which is then introduced into the fluctuating flow according to the Karman Pohlhausen approach. Using this method, separate solutions of fluctuating flow for small and large frequencies are obtained. Lighthill's approach is extended to the case of traveling waves with varying propagation speeds [6]. Results indicate large effects of the traveling wave velocity on fluctuations inside the boundary layer.

Telionis and Romaniuk [3] extend Lighthill's approach to include a third streaming term in addition to mean and fluctuating components. With the addition of the energy equation, streaming

Contributed by the Heat Transfer Division of ASME for publication in the Journal of Heat Transfer. Manuscript received July 14, 2019; final manuscript received October 14, 2019; published online December 9, 2019. Assoc. Editor: Sara Rainieri.

is calculated for both velocity and temperature fields in a linearly accelerating flow with temporal disturbances imposed at the freestream and inlet. Significant thermal streaming effects are noted, and the streaming is shown to be a strong function of the frequency parameter. However, the research effort does not attempt to isolate the effect of freestream fluctuations from the acceleration of the mainstream flow.

With the advancement of modern computational fluid dynamics tools, higher order analysis of the problem has been considered. Initially, periodic external perturbations and their aero-thermal impact on turbulent structures have been studied by unsteady Reynolds Averaged Navier Stokes (URANS). The effect of Prandtl and Strouhal numbers on the heat flux oscillations is analyzed [7]. In two-dimensional (2D) evaluations, transient heat flux is shown to be a strong function of thermal to momentum boundary layer thickness ratios [8]. Through the ability to cope with growing computational cost, large Eddy simulation and direct numerical simulation (DNS) investigations are conducted for an incompressible channel flow with pulsating pressure gradient over a range of excitation frequencies [9]. Having a smaller Stokes layer thickness that lies within the viscous sublayer, higher excitation frequencies do not affect the turbulent structures considerably. Therefore, the lower frequency pulsations are demonstrated to be more conducive to flow modulation. Furthermore, in an attempt to identify the relevant coherent structures in an oscillatory boundary layer, DNS analysis is performed [10] and streaks/structures inside the inner wall layers are found to have frequency double the freestream oscillations. In the presence of highly unsteady instantaneous flow features, as the temporally averaged heat transfer does not necessarily directly correlate with time-mean aerodynamic fields due to different time scales, the subsequent impact on local surface heat exchange is not obvious. Moreover, among the few works focusing on numerical heat transfer simulations in the presence of pulsatile flow [11], no significant impact is seen on time-averaged temperature profiles with or without excitations.

Due to small spatial scales, and the presence of solid–fluid interface, the experimental data are generally scarce for streaming under nonzero mean flow conditions. Focusing only on the aerodynamic part, turbulent oscillating boundary layers are studied through experiments [12–14] and the presence of Stokes layer is identified. However, only two studies (Hill and Stenning [15], Patel [6]) provide information about the fluctuating flow amplitude and phase in laminar flow. Comparing the Lin [5] and Lighthill [2] solutions with experimental results [15], good correlation is observed in high frequency temporal oscillations. For low frequencies temporal oscillations, experiments match calculations of Lighthill [2] and Nickerson [16]. However, for intermediate frequencies, calculations do not match well with the data. Later, in an attempt to imitate a traveling wave disturbance, vortices from oscillating flaps are used to perturb flow over a flat plate by Patel [6]. It is observed that the phase of oscillations near the wall differs significantly from the phase in the freestream. However, his calculations do not match well with the experiments performed. Moreover, the experimental literature studying the effect of streaming on forced convection is rather inconclusive due to the scattered, and conflicting findings. Some studies present a notable augmentation in heat transfer [17–21], whereas others demonstrate a detrimental or negligible influence [22–27].

1.1 Motivation. Building upon the existing scientific literature, streaming in nonzero mean flows introduces additional gradients to the solid–fluid interface under specific conditions. If implemented adequately to forced convection problems, this introduces the possibility to enhance or reduce heat transfer on attached aero-thermal boundary layers. However, the small spatial scales and the inherent unsteady nature of streaming has presented challenges for both experimental and numerical investigations, preventing fundamental understanding. In order to develop the adequate tools that will enable the identification of dominant aero-thermal streaming mechanisms, a new numerical approach is necessary to simulate the fluctuating flow with various of degrees of fidelity. Along these lines, three complimentary numerical abstraction levels are considered.

First, high-order DNS simulations are considered to fully characterize the temporal evolution of fluctuations and their interaction with the turbulent flow in the compressible regime. However, these calculations are computationally expensive and therefore, the streaming flow is modeled with U-RANS, estimating the aggregate impact on forced convection. Because the streaming phenomenon is a function of numerous flow and fluctuation parameters, URANS is too costly for conducting large-scale parametric investigations. Therefore, for rapid and economical exploration of heat transfer modulation as a function of various flow and fluctuation parameters, a laminar model is developed to calculate streaming over a flat plate adhering to laminar boundary layer theory and absent of any additional assumptions.

In the scope of this paper, the three numerical models with varying degrees of abstractions are presented, with exemplary results. This numerical framework paves the way toward improved understanding of physics, as well as toward the identification of optimal parameter space for heat transfer enhancement and reduction.

2 Numerical Framework

This section provides details of numerical methods used for calculation of streaming and fluctuating flows.

2.1 Direct Numerical Simulation. The general Navier–Stokes equations governing a compressible, unsteady flow can be written as

$$\begin{aligned} \frac{\partial \rho}{\partial t} + \frac{\partial}{\partial x_i}(\rho u_i) &= 0 \\ \frac{\partial \rho u_i}{\partial t} + \frac{\partial}{\partial x_j}(\rho u_i u_j) &= -\frac{\partial p}{\partial x_i} + \frac{\partial \sigma_{ij}}{\partial x_j} + f_i \delta_{1i} \\ \frac{\partial E}{\partial t} + \frac{\partial}{\partial x_j}\left[(E+p)u_j\right] &= -\frac{\partial q_j}{\partial x_j} + \frac{\partial}{\partial x_j}(u_i \sigma_{ij}) + f_i u_i \delta_{1i} \end{aligned} \tag{1}$$

where ρ, u_i, and p represent density, velocity and pressure, respectively, and total energy E, viscous stress tensor σ_{ij}, and heat flux vector q_j are defined as follows:

$$\begin{aligned} E &= \frac{p}{\gamma - 1} + \frac{1}{2}\rho u_i u_i \\ \sigma_{ij} &= \frac{\mu}{Re}\left(\frac{\partial u_i}{\partial x_j} + \frac{\partial u_j}{\partial x_i} - \frac{2}{3}\frac{\partial u_k}{\partial x_k}\delta_{ij}\right) \\ q_j &= \frac{\mu}{Re\,Pr}\frac{\partial T}{\partial x_i} \end{aligned} \tag{2}$$

In DNS, these equations are solved along with the perfect gas equation. The CFDSU code, originally developed at Stanford University, has been modified in-house at Purdue University. Discretized using the sixth-order compact finite difference method, a staggered grid is implemented to enhance the numerical stability as well as accuracy [28]. Time advancement is carried out by third-order Runge–Kutta method.

Since there has been no prior study to assess the validity of large Eddy simulation subgrid-scale models to simulate the pulsating compressible flows, we have avoided employing this technique and relied only on the DNS results.

2.2 Two-Dimensional Unsteady Reynolds Averaged Navier Stokes. As an intermediate fidelity simulation, URANS is conducted in a numerical domain, consisting of an isothermal flat

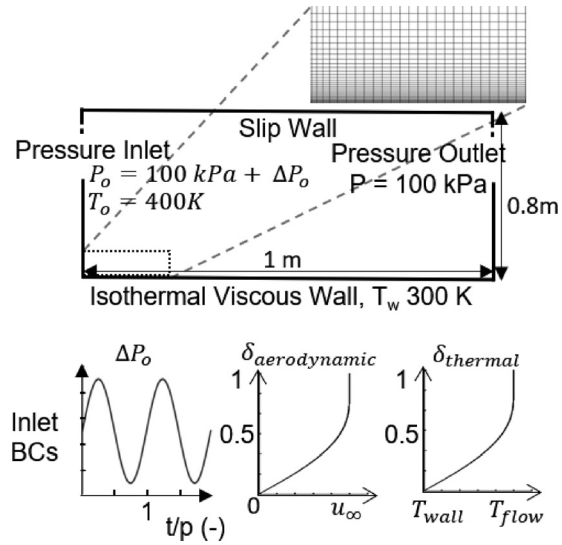

Fig. 1 Two-dimensional URANS domain and boundary conditions for a flat plate

plate at 300 K of 1 m length, sketched in Fig. 1. The URANS and finite volume simulations are evaluated with the solver ANSYS FLUENT taking advantage of the laminar model and the k-omega Menter's shear stress transport (SST) model for the turbulent simulations. The working fluid is air, which is modeled as an ideal gas, the Sutherland law accounts for the effect of the temperature on the molecular viscosity. Total pressure and total temperature boundary conditions are imposed at the inlet of the domain. The acoustic excitation is enforced through inlet total pressure fluctuations that model the discharge of compression and expansion waves. At the trailing edge of the plate, the static pressure is settled through a pressure outlet boundary condition, mimicking the discharge of the flow to a constant pressure reservoir. The static pressure outlet boundary condition models the discharge of the flow to a constant pressure reservoir. At the outlet of the domain, the compression waves are reflected as expansion waves. This representation is similar to a wind tunnel experiment where the trailing edge of the plate coincides with the outlet plane of a test section, where the flow is exhausted to atmosphere or vacuum.

The upper boundary of the domain is modeled as a slip wall without penetration, $u = U_\infty$ and $v = 0$. The height of the domain is at least 100 times larger than the boundary layer displacement thickness, ensuring a negligible impact of the upper boundary on the flow evolution near the wall, as well as the heat flux distribution.

Cantilevered and developed boundary layer flat plate configurations are considered. In the cantilevered plate case, the boundary layer develops from the inlet of the domain, which is the leading edge of the plate. On the other hand, for the developed boundary layer case, the incoming momentum boundary layer follows a Paulhalsen profile and the thermal boundary layer is derived from the Crocco relation, as depicted in Fig. 1.

The k-omega SST turbulent model is selected for the turbulence closure. Consisting of a blend between the $k-\epsilon$ for the mean flow (the most reliable turbulence model for the freestream flow) and the $k-\omega$ for the near wall region (with proven reliability in resolving the shear stress and heat flux). In a wide range of Reynolds and Mach numbers, the superior performance of k-omega SST in resolving the wall fluxes in attached flow conditions is demonstrated [29]. The URANS simulations assume fully turbulent behavior from the leading edge of the plate and therefore, no transition model is required. The time-step and inner iterations are selected based on a benchmark analysis resolving at least 4000 time steps for each period of excitation and with 20 inner iterations to ensure temporal convergence. Second-order upwind schemes are employed for the flow and turbulent kinetic energy and second-order implicit methods are used for the temporal formulation.

The numerical domain is meshed with ANSYS ICEM following a blocking strategy. The methodology outlined in Ref. [30] is employed to ensure the correct spatial discretization and guarantee that the results are mesh independent. Six different discretization approaches are evaluated at steady-state conditions, $U_\infty = 80\,\mathrm{m/s}$, $P_o = 100\,\mathrm{kPa}$ and $T_\infty = 400\,\mathrm{K}$. The cell count ratio between each mesh (finer/coarse) is 1.4, with a fixed aspect ratio. For all the different mesh configurations, Fig. 2 presents the wall shear stresses and the momentum boundary layer thicknesses at the plate midcord. The grid convergence index of the mesh of 200×1600 elements is about 0.02, guaranteeing proper spatial resolution. The grid convergence index characterizes the change in the value of a reference variable with respect to a change in mesh size. A low grid convergence index implies that further mesh refinement will only provide minimal improvements. The boundary layer thickness and the axial wall shear stress deviate less than 0.5% when compared to the results from the finer meshes. Hence, this level of spatial discretization is sufficient to guarantee the proper numerical resolution.

2.3 Development of Laminar Numerical Tool for Streaming. As a fast numerical tool for parametric optimization, a new laminar approach to streaming calculations is developed in-house at IIT-Technion. For the calculations of streaming velocity over a flat plate, semi-analytical method proposed by Lin [5] is extended to traveling wave disturbances of various wave speeds.

Laminar boundary layer theory developed by Prandtl governs the velocity and temperature fields over a semi-infinite, isothermal flat plate geometry. When small amplitude fluctuations are superimposed, the flow is assumed to remain laminar and therefore the governing equations are the same. Pressure gradient term in the laminar boundary layer equation is replaced using the freestream velocity. The momentum and continuity equations governing the laminar boundary layer are segregated to mean and fluctuating parts. Assuming zero mean fluctuations, the resulting equation averaged over time can be written as [31]

$$\overline{u}\frac{\partial \overline{u}}{\partial x} + \overline{v}\frac{\partial \overline{u}}{\partial y} = \overline{U}\frac{d\overline{U}}{dx} + \nu\frac{\partial^2 \overline{u}}{\partial y^2} + \overline{U`\frac{\partial U`}{\partial x}} - \left(\overline{u`\frac{\partial u`}{\partial x}} + \overline{v`\frac{\partial u`}{\partial y}}\right) \tag{3}$$

The last three terms represent the nonlinear contribution of fluctuations to the mean flow, i.e., streaming. A correct estimation of this streaming requires a well resolved fluctuating flow. This can be obtained by subtracting the mean flow (Eq. (3)) from the boundary layer equation [5]

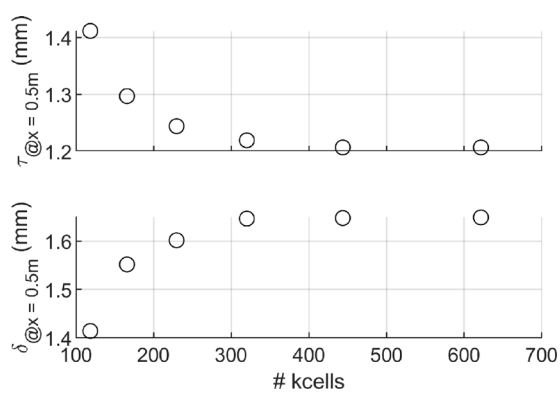

Fig. 2 Two-dimensional URANS domain mesh sensitivity analysis

$$\frac{\partial u'}{\partial t} - \nu \frac{\partial^2 u'}{\partial y^2} - \frac{\partial U'}{\partial t} = \left(\overline{U}\frac{\partial U'}{\partial x} - \overline{u}\frac{\partial u'}{\partial x} - \overline{v}\frac{\partial u'}{\partial y}\right) + \left(U'\frac{\partial \overline{U}}{\partial x} - u'\frac{\partial \overline{u}}{\partial x} - v'\frac{\partial \overline{u}}{\partial y}\right) + \left(U'\frac{\partial U'}{\partial x} - u'\frac{\partial u'}{\partial x} - v'\frac{\partial u'}{\partial y}\right) - \left(\overline{U`\frac{\partial U`}{\partial x}} - \left(\overline{u`\frac{\partial u`}{\partial x}} + \overline{v`\frac{\partial u`}{\partial y}}\right)\right) \quad (4)$$

where $\overline{u}, \overline{v}$, and u', v' are the mean and the fluctuating components of velocity, $\overline{U}$ and U' are the mean and fluctuating velocities at the freestream, x is the distance along the plate and y is the distance away from the plate. The x and y directions are nondimensionalized in terms of frequency parameter, $\xi = \omega x/U_\infty$, and Stokes layer thickness, $\eta = y/\sqrt{\nu/\omega}$, respectively. This detailed derivation can be found in Ref. [32].

Calculations are performed over a semi-infinite flat plate immersed in a uniform flow. Owing to parabolic nature of the governing equation for fluctuating flow, this can be accomplished with a finite domain, negating the need to specify a downstream boundary condition in the absence of reflections. Fluctuations in the form of traveling wave $U_o \sin(kx - \omega t)$ are imposed at the leading edge of the plate, where U_o is the amplitude, k is wave number, and ω is angular frequency of fluctuations. The spatial and temporal grid sizes are determined considering numerical stability requirements, Stokes layer thickness, and wavelength of traveling wave. The discretization in the transverse direction is fixed to a fraction ($\sim$1/10) of Stokes' layer thickness and the temporal discretization is selected according to the diffusive stability constraint. The streamwise discretization is then obtained from the Courant–Friedrichs–Lewy condition [33]. The numerical domain and the boundary conditions are shown in Fig. 3.

A second-order finite difference formulation is used to calculate mean flow over the flat plate using tridiagonal matrix algorithm [34]. The mean flow derivatives are approximated using second-order central difference and first-order upwind schemes in transverse and streamwise directions, respectively. A first approximation of mean flow is calculated without considering the nonlinear terms in Eq. (3). With this estimate, the fluctuating flow equation is solved using an explicit finite difference formulation in a predictive-corrective manner. For the fluctuating flow equation, forward first-order, upwind first-order, and central second-order discretization schemes are employed in the temporal, streamwise, and transverse directions, respectively. The initial estimate of fluctuating flow is analytically derived by solving the left-hand side of Eq. (4) for traveling wave disturbances. The estimate of fluctuating flow is then used to calculate the nonlinear contribution of fluctuations to the mean flow (last three terms in Eq. (3)). The process is repeated until the mean flow is converged.

The modified mean flow is then used to calculate the temperature fields using the unsteady energy equation governing the laminar flat plate boundary layer, written in terms of temperature as [31]:

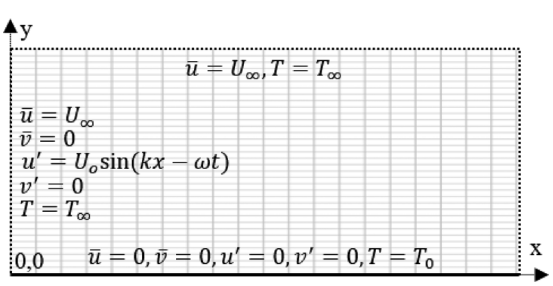

Fig. 3 Numerical flat plate domain for laminar analysis

$$\frac{\partial T}{\partial t} + u\frac{\partial T}{\partial x} + v\frac{\partial T}{\partial y} = \frac{k_f}{\rho c_p}\frac{\partial^2 T}{\partial y^2} + \frac{\nu}{c_p}\left(\frac{\partial u}{\partial y}\right)^2 \quad (5)$$

This equation is solved using a second-order finite difference formulation by tridiagonal matrix algorithm formulation. Similar to the mean flow, the mean temperature gradients are approximated using second-order central difference and first-order upwind schemes in the transverse and streamwise directions, respectively. Subsequently, the temperature field is used to calculate the heat transfer coefficient (h) and Nusselt number (Nu) of the iso-thermal flat plate, which is defined as

$$h = -\frac{k_f \left.\frac{\partial T}{\partial y}\right|_{y=0}}{T_o - T_\infty}, \quad N_u = \frac{hx}{k_f} \quad (6)$$

Therefore, change in convective heat transfer due to streaming is quantified using the ratio of N_u in the presence and absence of fluctuations, termed thermal enhancement factor (TEF). Similarly, the ratio of shear stress in the presence and absence of fluctuations is used to quantify the effect of streaming on shear stress, termed shear enhancement factor (SEF).

For laminar aero-thermal flow over a flat plate, this numerical approach captures the dependency of streaming on physical parameters; namely, mean flow velocity, thermal and aerodynamic properties of the medium, temperature of wall and the freestream, flow fluctuations amplitude, frequency, speed, and phase.

3 Validation

3.1 Direct Numerical Simulation for Fluctuating Flow Calculations. To assess the accuracy of this high-fidelity computational tool, computations are conducted to contrast the DNS findings with a benchmark case [35]. The compressible turbulent channel flow with isothermal walls is modeled in a computational domain of size $\Omega : L_x \times L_y \times Lz = 45.24 \times 7.2 \times 16.96$ mm and discretized by $N_x \times N_y \times N_z = 144 \times 128 \times 96$ elements. This resultant resolution is $(\Delta x^+, \Delta y^+_{\min}, \Delta z^+) \approx (19, 0.24, 10.7)$, based on the wall units where $y^+ = yu_\tau/\nu_w$, $u_\tau = \sqrt{\tau_w/\rho_w}$ and subscript w denotes the corresponding value at the wall. In these simulations, channel half width $\delta_h = 3.6$ mm, wall temperature, $T_w = 300$ K, and speed of sound at the wall are used as the references for length, temperature and, velocity, respectively. The corresponding Mach and Reynolds numbers are $M_b = U_b/c_w = 1.5$ and $\mathrm{Re}_b = \rho U_b \delta_h/\mu_w = 3000$, respectively. A forcing term is added to the right-hand side of the momentum and energy equations (Eq. (1)) which is adjusted at each time-step to keep the mass flowrate constant. Figure 4 illustrates the time-averaged streamwise velocity and normal Reynolds stresses components along with the data provided by Coleman et al. [35]. The results show an excellent agreement with the reference values.

For the current work, a subsonic channel flow with a relatively high Mach number has been considered. The channel has the same dimensions and discretization as the validation case. With periodic inlet and exit boundary conditions, the work focuses on the fully developed flow region. In the form of a temporal wave, acoustic excitation is applied on both spanwise side walls through a streamwise forcing term:

$$F_x(x, y, z, t) = A_f \exp\left(-10\frac{(x - x_m)^2}{L_{ls}}\right)\sin(\omega t) \quad (7)$$

where A_f, L_{ls}, and x_m are acoustic forcing amplitude, effective length of the excitation, and streamwise location of the maximum forcing with respect to the beginning of the channel. The computational setup is shown in Fig. 5

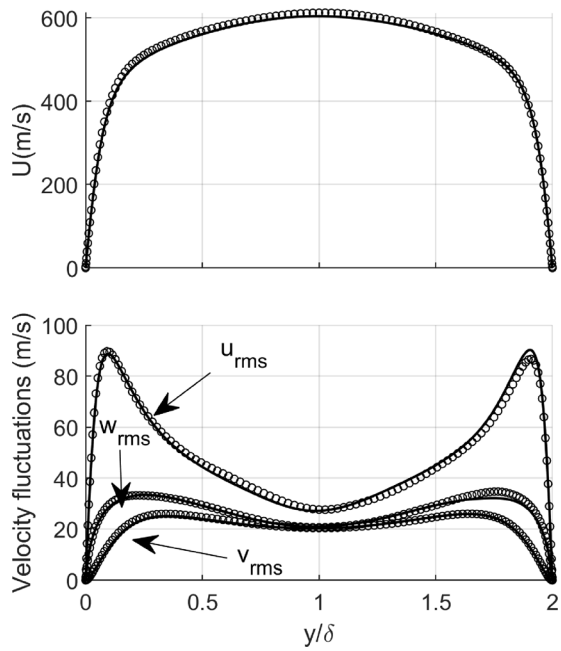

Fig. 4 Time-averaged streamwise velocity (top) and rms of fluctuation velocity components (bottom). Results of the present solver are shown in with solid lines while circles represent data provided by Ref. [35].

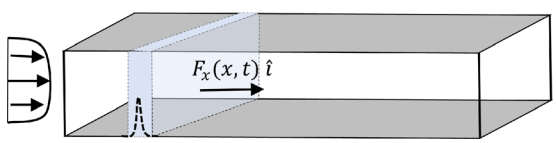

Fig. 5 DNS domain for fully developed channel flow with isothermal walls subjected to streamwise forcing

The time-resolved flow variables are decomposed into steady and unsteady components; the latter is further decomposed into "harmonic" and "random fluctuation" terms

$$q(x,t) = \underbrace{\overline{q(x)}}_{\text{steady term}} + \underbrace{\widetilde{q(\mathrm{x},\mathrm{t})}}_{\text{harmonic term}} + \underbrace{q'(\mathrm{x},\mathrm{t})}_{\text{random fluctuation}} \tag{8}$$

where the harmonic term is calculated following the phase-locked averaging of the instantaneous quantity:

$$\widetilde{q(\mathrm{x},\mathrm{t})} = \frac{1}{\mathrm{NT}}\sum_{\mathrm{n}=0}^{\mathrm{N}} q(\mathrm{x},\mathrm{t}+\mathrm{nT}) \tag{9}$$

3.2 Two-Dimensional Unsteady Reynolds Averaged Navier Stokes for Fluctuating Flow Calculations. In order to verify the performance of the selected numerical method over viscous, periodically excited flows, the Stokes second problem is considered as a test case. When the plate is oscillating at a velocity $u(0,t) = U_0\cos(\omega t)$ and stagnant freestream flow is $u(\infty,t) = 0$, the analytical solution is provided by

$$u(y,t) = U_0 e^{-\eta}\cos(\omega t - \eta) \tag{10}$$

In this case, the plate velocity amplitude and the excitation frequency are set at 10 m/s and 100 Hz, respectively. Figure 6(*a*) depicts the numerical domain and its setup for the validation case and Fig. 6(*b*) shows the momentum boundary layer profile for both numerical and analytical solutions at several time steps. The excellent agreement verifies the applicability of the presented numerical approach to study oscillatory flow behavior.

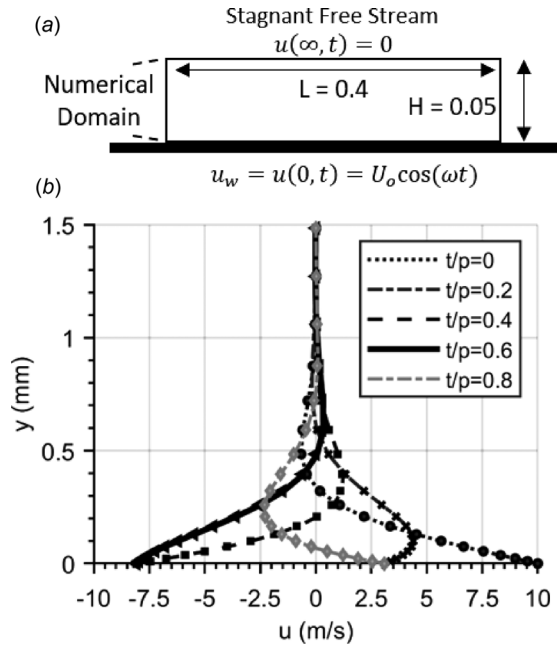

Fig. 6 URANS verification based on Stokes second problem (current methodology (lines), Analytical (markers))

3.3 Laminar Model for Fluctuating Flow Calculations. To validate the laminar model, experiments of Patel [6] are utilized, which is a unique experimental dataset providing boundary layer response to traveling wave disturbances. The data stems from experiments performed in a mean flow of $U_\infty = 10\,\mathrm{m/s}$, over which fluctuations of 5.6% amplitude ($U_0 = 0.56\,\mathrm{m/s}$, 140 dB) are superimposed at a frequency of $f = 10\,\mathrm{Hz}$. Although the velocity of disturbance is quoted to be 0.77 times the mean flow velocity, this is later corrected to 0.6 by Evans [36], resulting in a disturbance velocity of $Q = 6\,\mathrm{m/s}$.

Figure 7 compares amplitude and phase obtained from the laminar model and these experiments, as well as Patel's numerical solution. The amplitude of fluctuations starts from zero at the wall, increases to a value more than unity at about 1.5 Stokes layers, oscillates to less than unity at a distance of 3.5 layers, and finally settles at unity. The laminar model follows the overall experimental profile of the fluctuation amplitude, significantly better than numerical analysis of Patel [6], which is an extension of Lighthill's approach [2]. Patel's numerical approach failed to predict correct amplitude of fluctuations due to omission of several terms from Eq. (4). Specifically, Patel [6] modeled the first

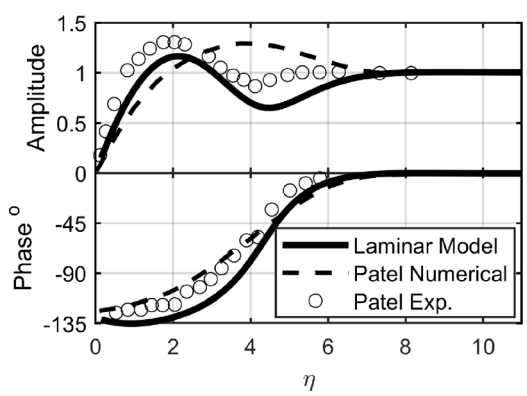

Fig. 7 Comparison of fluctuating velocity amplitude and phase calculated by laminar model to the experiments and calculations performed by Patel [6]

Table 1 Comparison of computational costs required by different numerical approaches for fluctuating flow calculations

Approach	CPU hours per unit volume for: Single oscillation period	CPU hours per unit volume for: Converged solution
DNS	5.8×10^6	3×10^8
URANS (2D finite volume)	35	1×10^3
Laminar model	4	4×10^1

two terms on the right-hand side of the equation whereas the last six terms were neglected from the fluctuating flow calculations. However, the magnitude of three of these last terms becomes significant for greater than unity values of U_∞/Q, and therefore, should not be ignored.

3.4 Comparison of Computational Costs. Table 1 compares the computational costs of the presented numerical approaches. Although the details of each simulation, including the physical parameters, numerical methods, and computational hardware employed, are not the same, this table can provide a qualitative comparison between the different methods. The cost of URANS calculations is almost independent of the Reynolds number [37]. For the computational setup shown in Fig. 1, approximately 35 CPU-hours were required to perform calculations for one excitation period. These simulations were carried out on the Rice cluster of Purdue University consisting of two 10-core Intel Xeon-E5 processors and 64 GB of memory. Unlike this approach, DNS calculations become increasingly more expensive at higher Reynolds numbers at a rate of Re3. Therefore, DNS of the computational setup shown in Fig. 1 needs approximately 5.8×10^6 CPU-hours per cycle. Laminar model, on the other hand, is orders of magnitude faster than both aforementioned calculations, where only 4 CPU-hours are required to simulate a single oscillation period. Moreover, the number of periods required for convergence are 50, 30, and 10, respectively, for DNS, URANS, and laminar model. This further accentuates the differences in computational costs of the three numerical approaches.

4 Results

4.1 Direct Numerical Simulation of Streaming in Compressible Channel Flow. Direct numerical simulation computations are performed in the fully developed channel flow at $M_b = 0.75$, $T_w = 300\,\mathrm{K}$, and $\mathrm{Re}_b = 3000$, for the domain shown in Fig. 5. Here, domain has the size $\Omega : L_x \times L_y \times Lz = 74.6 \times 11.88 \times 28\,\mathrm{mm}$ which is discretized by $N_x \times N_y \times N_z = 144 \times 128 \times 96$ elements leading to a dimensionless grid spacing (based on wall units) similar to the validation test case. The acoustic forcing amplitude is set to $A_f = 0.038\mathrm{N}$, and following Yao et al. [38], it can be represented by $A_f^+ = A\mu/u_\tau^3$ where in the present case $A_f^+ = 0.458$. The effective length of the excitation is assumed to be $L_{ls} = 12.5\,\mathrm{mm}$ and streamwise location of the maximum forcing is $x_m = 0.45\,\mathrm{mm}$. The time-step is chosen such that the acoustic Courant–Friedrichs–Lewy is maintained below 0.2.

Excitation frequency ω is chosen based on linearized Navier–Stokes equations, discretized using a Chebyshev spectral method absent of any external excitations [39]. Time-averaged velocity and temperature fields are chosen as the base flow quantities. The eigenvalue spectrum associated with the largest wavelength in the domain is shown in Fig. 8.

The horizontal axis represents the real part of the eigenmodes, which identifies the angular velocity, whereas the vertical axis displays the corresponding growth rate. Without external excitation, all modes have negative growth rate, and are therefore stable. In this case, the optimal frequencies for acoustic excitation are selected to be the two least stable modes, which are the ones

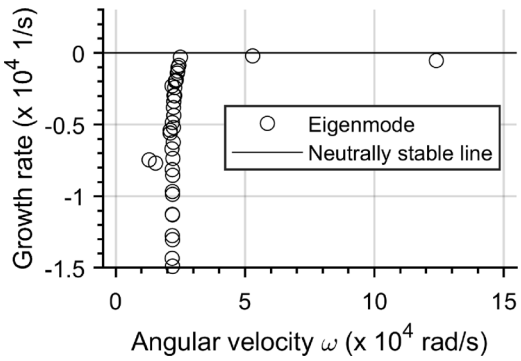

Fig. 8 Eigenvalue spectrum associated with largest wavelength in the domain

closest to the neutrally stable line, $f_1 \sim 8.4$ kHz and $f_2 \sim 16.8$ kHz. In the present case $f_2 \sim 2f_1$, but at higher Mach numbers this does not necessarily apply.

For an excitation frequency corresponding to the least stable mode f_1, Fig. 9 shows the harmonic component of spanwise-averaged flow temperature at four different phases in a period. The walls are depicted in top and bottom of each chart. The first phase snapshot is captured when the excitation magnitude at the inlet is maximum. This is reflected as a highly positive island in the most left portion of the domain. With the advection, the temperature maps contain the footprint of acoustic waves interacting with the turbulent structures, evidenced by formation of rollers, with different sizes and strengths. Downstream of each roller, a wake region exists containing smaller rollers with different frequencies which appear due to nonlinear interactions. The existence of these rollers significantly disturbs the near wall structures of the turbulent boundary layer.

The direct aero-thermal alteration on the walls caused by the streaming is shown in Fig. 10 for the selected frequencies. Surface averaged thermal and shear enhancement factors are charted over 50 periods, and each point represents a running average of the temporal history. For each excitation frequency, the temporal evolution of $\overline{\mathrm{SEF}}$ closely follows the trend of $\overline{\mathrm{TEF}}$. Both quantities experience a decay within the first few periods of excitation, followed by a rise in their values around which they oscillate. The

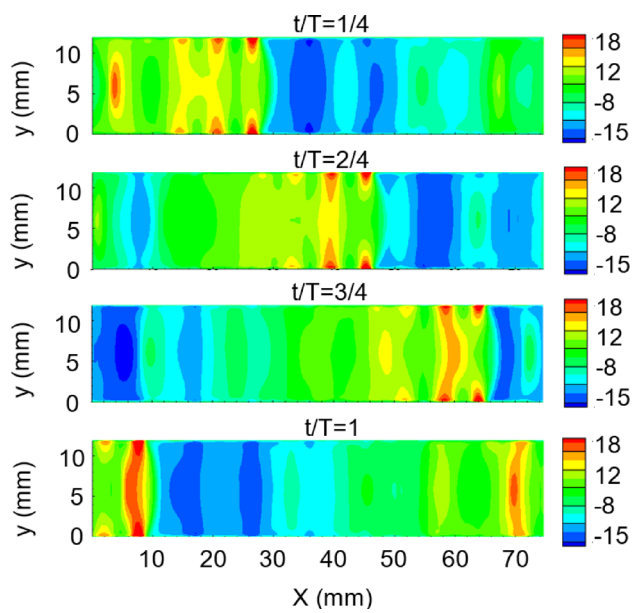

Fig. 9 Harmonic component of temperature field at four phases of the excitation period at $f = 8.42$kHz

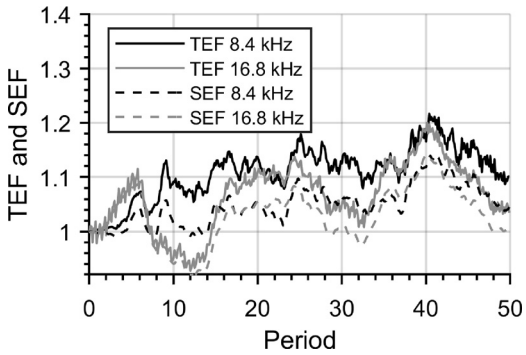

Fig. 10 Spatial averaged temporal history of aggregate shear and TEFs

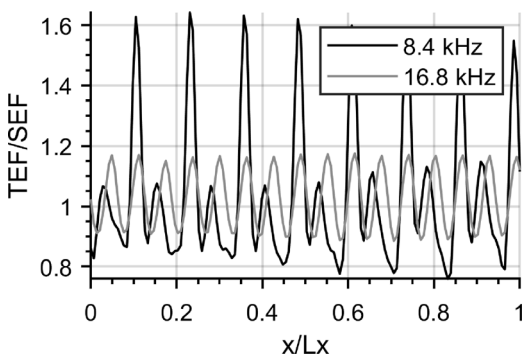

Fig. 11 Spatial distribution of TEF/SEF at 8.4 kHz and 16.8 kHz, time-averaged over 50 cycles

time required to reach the quasi-steady level appears to be directly proportional to the frequency. For both frequencies, the rise in heat transfer ($\overline{\mathrm{TEF}}$) is larger than that of shear ($\overline{\mathrm{SEF}}$). This suggests a deviation from Reynolds analogy, indicating an impact beyond roughness. Both frequencies reflect similar $\overline{\mathrm{SEF}}$ of 5% order, indicating the same level of increased pressure loss across the surface due to the excitations. However, the case with lower frequency results in a higher heat transfer enhancement of 12%, whereas the enhancement of the higher frequency is limited to 6%. This is consistent with the prior purely aerodynamic streaming studies [9] that suggest an inversely proportional impact of frequency on streaming.

Figure 11 illustrates the spatial distribution of TEF/SEF time-averaged over 50 cycles at two different excitation frequencies. While the Reynolds analogy suggests TEF/SEF to be one across the domain, regions with significantly higher or lower values can be observed in the present simulations. This indicates a phenomena different than simple introduction of roughness, and that Reynolds analogy does not represent the physics of the phenomena. This ratio in the high frequency case simply oscillates around the unity, whereas the lower frequency configuration shows a greater deviation from unity and hence the Reynolds analogy, up to 60%.

4.1.1 Comparison of Direct Numerical Simulation and Unsteady Reynolds Averaged Navier Stokes in Calculation of Streaming in Turbulent Compressible Channel Flow. To analyze the applicability of a reduced fidelity model in simulating the acoustic excitation of turbulent flows, a case similar to the one described in Sec. 4.1 is tested using both URANS and DNS methods. The excitation frequency is set to $f \approx 8.2$ kHz and the forcing amplitude (A_f) has been reduced by a factor of 2 in order not to surpass the numerical stability of the solver. In the first step, the base flow quantities obtained using these two approaches are compared in Fig. 12.

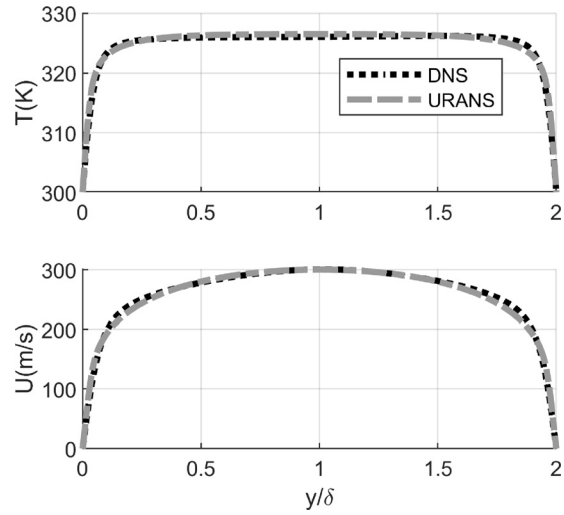

Fig. 12 Baseflow comparison for DNS and URANS numerical model

The findings of streamwise velocity and temperature distribution across the channel height are in a good agreement, thereby indicating the adequacy of the URANS solver for resolving the overall flow topology.

In the next step, we analyze the system response to the acoustic forcing in the near wall region. To isolate the effect external perturbations on the system we defined the temperature fluctuations as

$$\delta T(t) = T_{\mathrm{exc}}(t) - T_{\mathrm{base}}(t) \tag{11}$$

where $T_{\mathrm{exc}}(t)$ and $T_{\mathrm{base}}(t)$ represent the temperature for a specific location at time t in the excited case and base flow simulations, respectively. DNS and URANS cases start from the same initial condition and have the same spatial and temporal resolution.

Figure 13 depicts the evolution of these temperature fluctuations, normalized by its maximum value throughout the excitation process. Evidently, the URANS approach is able to capture the macroscopic effect of the acoustic streaming, where the impact of the mean flow conditions oscillations is reflected on the near wall region by means of increased shear and temperature gradients. However, the URANS models cannot capture the impact of the acoustic oscillations on the turbulent structure's disruption and its ramifications on the turbulent dissipation or enhancement. Therefore, URANS can only be used as a tool for guiding higher fidelity simulations to the adequate parameter space, for which the physical phenomena can be studied using DNS.

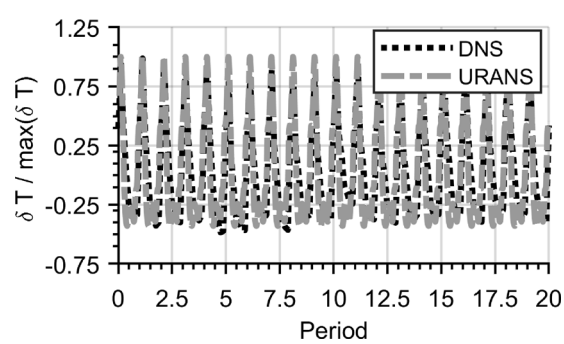

Fig. 13 Referenced temperature fluctuations at $y+ = 4$, URANS versus DNS results

4.2 Unsteady Reynolds Averaged Navier Stokes Simulation of Streaming Over Flat Plate. To assess whether the computational complexity can be reduced in characterizing streaming, URANS calculations are performed over a turbulent and laminar flat plate for the domain presented in Fig. 1. For each selected case, to identify the impact of the acoustic excitation on wall flux, separate simulations are performed with and without excitation. The base flow is imposed with the following inlet boundary conditions: $P_o = 102.815\,\text{kPa}$, $T_0 = 400\text{K}$, and $P = 100\,\text{kPa}$. This results in a freestream velocity of $U_\infty = 80\,\text{m/s}$. The simulations of the steady-state conditions are considered converged once the residuals decay below 10^{-7} and once the oscillations or changes on the shear stress and heat flux are below 0.1% of the actual mean value. The periodic convergence of the acoustically excited cases is ensured following the approach outlined by Clark and Grover [40].

For a laminar cantilever flat plate subjected to 50 Hz total upstream pressure fluctuations, shear stress and heat flux are evaluated for perturbation amplitudes of 200, 600, and 1000 Pa. Figure 14 shows that across all amplitudes, both the SEF and TEF reflect an initial decrease, followed by a gradual increase to the nominal value of 1. Moreover, as the excitation amplitude increases, the extent of this modulation is intensified.

For a fixed amplitude 600 Pa (ΔP_o), the frequency of fluctuations is varied from 1 Hz up to 800 Hz. Figure 15 reflects the corresponding shear and thermal enhancement factors for several frequencies. For low frequencies (1–100 Hz), a reduction in heat flux and shear stress is observed, further isolating the mean flow from the wall. At 200 Hz, there is heat transfer enhancement near the leading edge of the plate and a heat flux reduction toward the outlet of the domain.

A similar behavior is observed for the shear stresses, with an increased drag for the first half of the spatial domain, followed by a reduction. As the frequency is further increased, the peaks of maximum and minimum heat transfer are reduced, and the impact of the excitation is attenuated.

The excitation frequency of 200 Hz provides higher local enhancement and reduction as compared to other frequencies. This is an artifact of the domain acoustic response. The pressure changes across the domain are transmitted following the fastest flow characteristic. Once a pressure wave is released, it travels at the speed of sound plus the streamwise flow velocity, $(c + U_\infty)$. When this wave reaches the outlet of the domain, it is reflected as an expansion wave that travels upstream at a speed of $(c - U_\infty)$. The actual time that a pressure wave will take to commute across the domain and bounce back will then be defined by $L/(c + U_\infty) + \text{L}/(c - U_\infty)$, which is about 5 ms for this domain. It leads to a domain frequency response of 200 Hz. When the domain response and excitation frequencies match, a standing wave is generated increasing the amplitude of oscillations fourfold at the antinodes.

For the 200 Hz case, the effect of the inlet condition is assessed by altering the upstream aerodynamic boundary layer thickness from 0 (cantilever) to 1 mm, 2 mm, and 4 mm. For an oscillation amplitude of 600 Pa, Fig. 16 shows the variation of SEF and TEF along the plate. For all laminar conditions, there seems to be a positive correlation between the upstream boundary layer thickness and thermal streaming enhancement factor. For the case of 4 mm inlet boundary layer thickness, a heat transfer enhancement

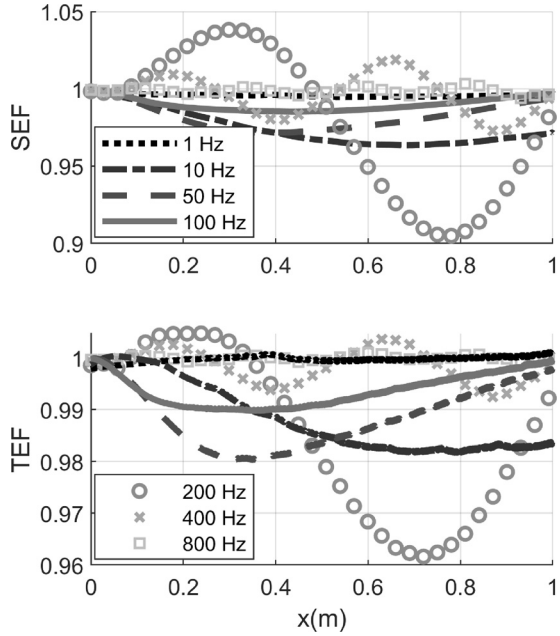

Fig. 15 Integral effect of acoustic excitation on cantilever flat plate at several frequencies and at a constant amplitude of 600 Pa over the shear stress and heat transfer distribution

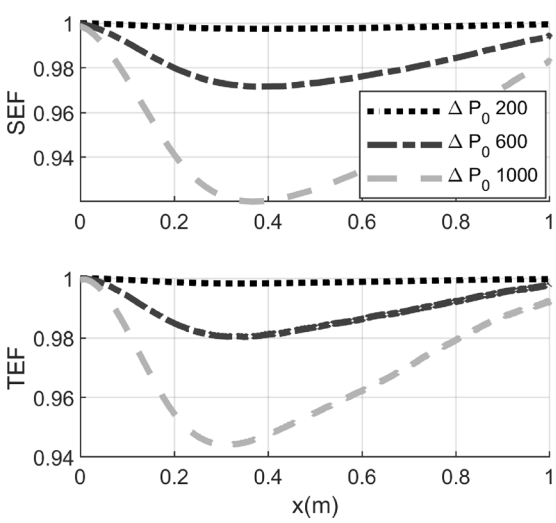

Fig. 14 Excitation amplitude impact on the shear stress and heat transfer modulation over cantilever laminar flat plate for a constant frequency of 200 Hz

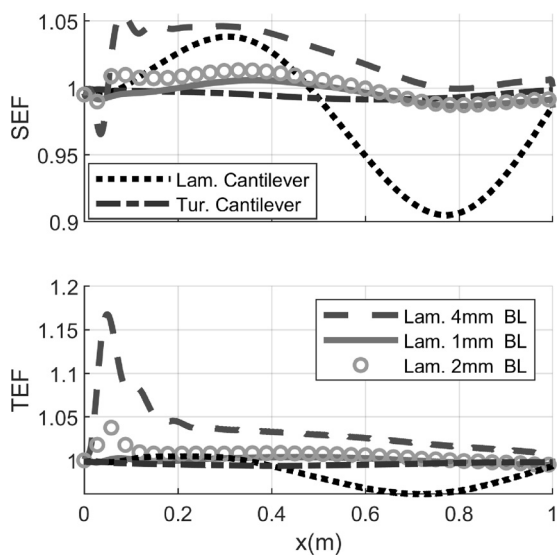

Fig. 16 Shear stress and heat transfer evolution for laminar and turbulent cantilever evaluations versus incoming boundary layer cases based on an excitation frequency of 200 Hz and an amplitude of 600 Pa

of up to 15% is achieved with shear penalty increase of 5% only. Moreover, unlike the cantilevered beam, the modulation persists across the entire domain while decreasing in magnitude in the streamwise direction due to the thickening of the unexcited thermal boundary layer. For the turbulent case, the impact of the acoustic excitation is negligible for this amplitude. This is thought to be associated with the already large aero-thermal flow gradients being present near the wall.

Figure 17 represents the ratio of heat transfer and shear stress enhancements for cantilevered laminar and turbulent cases, as well as for developed incoming boundary layers. Based on the Reynolds analogy, the heat transfer signature should follow the trend prescribed by the shear enhancement. This would result in the charted quantity remaining at a level of unity. However, we can notice that for all the cases analyzed in this framework, under acoustic excitation, the trend of the heat transfer enhancement deviates from the shear stress (locally up to 20%), reflecting once again on the failure of Reynolds analogy to describe the heat transfer in periodically excited flow.

Figure 18 illustrates the thermal enhancement for cantilever flat plate cases for laminar and turbulent conditions at 200 Hz excitation. The results of the laminar case with an amplitude of 600 Pa are compared with the results of the turbulent case at 600 and 2000 Pa. The trend of the turbulent cases deviates from the laminar results, indicating that there might be different mechanisms affecting the streaming for laminar and turbulent conditions. Figure 18 bottom, represents the referenced thermal enhancement where the actual enhancement is divided by the maximum enhancement over the plate. By scaling the thermal enhancement,

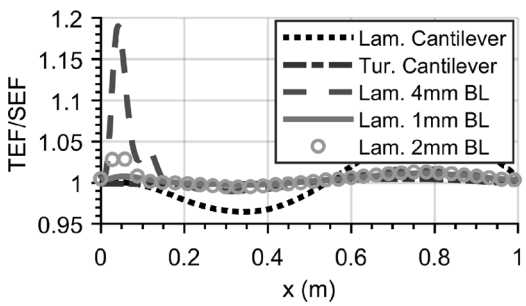

Fig. 17 Ratio between thermal and shear enhancement for cantilever laminar, turbulent flat plates and developed incoming boundary layers

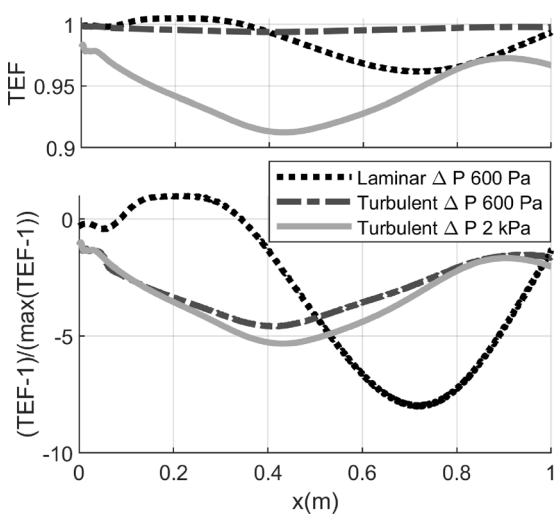

Fig. 18 Thermal enhancement and relative thermal enhancement for laminar and turbulent cases at 200 Hz excitation

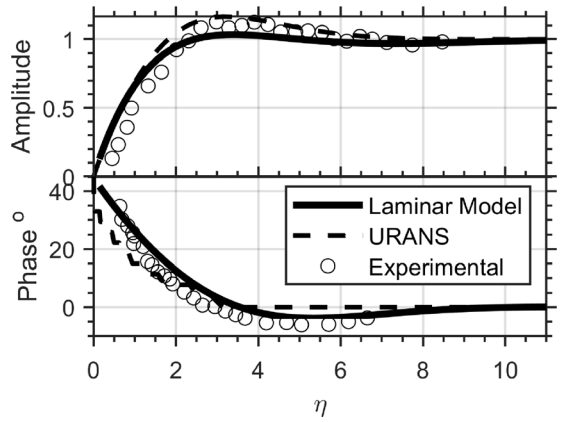

Fig. 19 Comparison of the fluctuating velocity using the laminar model, finite volume solver, and experiments [15]

we can observe that the trend obtained for the turbulent cases remains almost unaltered by the actual magnitude of the oscillation.

It is understood that laminar and turbulent boundary layers may not always respond similarly to flow modulations. This is because the two type of boundary layers have different profiles except in a very small region close to the wall (laminar sublayer for the turbulent flow), and their interaction with the Stokes' layers may be different. Nevertheless, as we see in Figs. 6 and 7, the effect of fluctuations is observed only for few multiples of Stokes' layer thicknesses. Therefore, if laminar sublayer thickness of a turbulent flow is of the same order as Stokes' layer thickness, then similar impact of modulations can be expected on both turbulent and laminar boundary layers. This constitutes the motivation for further reducing the fidelity to a purely laminar solver for a subset of the parameter space, decreasing the computational cost.

4.3 Laminar Model of Streaming Over Flat Plate. Fluctuating velocity calculated by the newly developed streaming model can be contrasted with the finite volume solver computations. For a flow over a flat plate with freestream velocity of 20 m/s, oscillations of 3 m/s amplitude are imposed at 150 Hz. Figure 19 presents the amplitude and phase of fluctuations at a streamwise location of 0.1 m, as a function of normalized distance from the wall. Moreover, there exists experimental results from Hill and Stenning [15] for this particular set of parameters, which corresponds to $\xi \sim 4.9$ in their notation.

The amplitude of fluctuations starts from zero at the wall, increases to a value more than one at a distance of three Stokes layers, and then decreases to unity. Fluctuations at the wall are about 45 deg out of phase with respect to the freestream. The solution provided by the laminar model is validated via excellent agreement with both the URANS simulations, as well as the experimental data. The very slight differences are likely associated with the propagation velocity of the temporal disturbance being infinite for the experiments, and speed of sound for the URANS and laminar model calculations.

Having established the validity of the laminar model for flow fluctuations, their streaming manifestations are analyzed Fig. 20. The streaming velocity magnitude ranges up to 1 m/s, opposing the mainstream flow. For a flow temperature of 300 K and a wall temperature of 360 K, the corresponding streaming temperatures are ~3 K. This increase in flow temperature stems from the decrease in mean flow velocity close to the wall. This is manifested as a 10% drop in local heat transfer with a 20% drop in shear, as presented in Fig. 21.

The newly developed laminar model allows for rapid and economical calculations of heat transfer for various combinations of flow and fluctuation parameters over the flat plate. For example, a

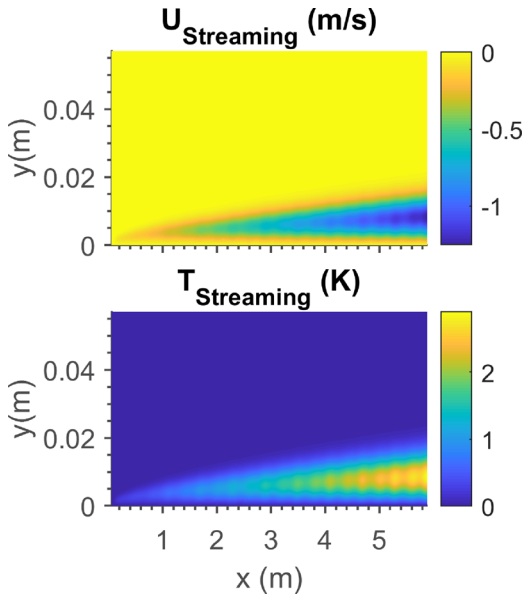

Fig. 20 Streaming velocity and temperature for $Q = 6$ m/s, $U_o = 0.56$ m/s, $U_\infty = 10$ m/s, and $f = 10$ Hz

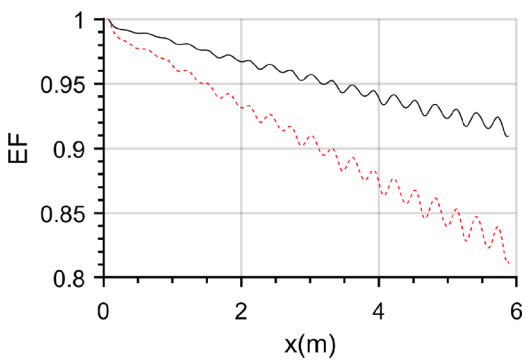

Fig. 21 Thermal (-----) and shear (- - -) enhancement factors for a traveling wave disturbance over a flat plate under $Q = 6$ m/s, $U_o = 0.56$ m/s, $U_\infty = 10$ m/s, and $f = 10$Hz

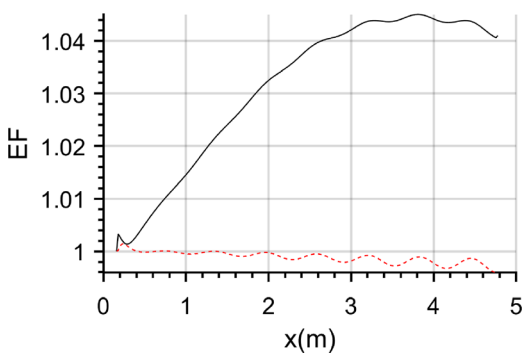

Fig. 22 Thermal (-----) and shear (- - -) enhancement factors for a traveling wave disturbance over a flat plate under $Q = 12.5$ m/s, $U_o = 0.5$ m/s, $U_\infty = 10$ m/s, and $f = 10$ Hz

change in disturbance velocity (Q) and amplitude of fluctuations (U_0) to 12.5 m/s and 0.5 m/s, respectively, leads to a positive heat transfer enhancement of 4%, with no change in shear, as shown in Fig. 22, reflecting once again on the failure of the Reynolds analogy.

5 Summary and Conclusions

The present research describes the development of a three-tier numerical approach, intended to capture the complex aero-thermo-acoustic flow physics of acoustic streaming with various degrees of fidelity. Hence, the presented numerical framework enables the optimization of the parameters conducive to a heat transfer enhancement with reduced pressure losses.

As the first tier, direct numerical simulations are used to investigate the effect of traveling-wave acoustic excitation on the turbulent structures in a wall-bounded compressible flow. Linear stability analysis is exploited to find the optimal frequencies. Under these conditions, newly formed spanwise-correlated vortices interact with the classic near wall turbulent structures and eventually lead to modification of the mean flow quantities in the near wall region only. Moreover, the value of heat transfer enhancement does not follow increase in skin friction (as seen in the results from DNS, URANS, and laminar model alike), thereby disobeying Reynolds analogy. This shows that streaming phenomenon behaves differently than introduction of roughness into flow passages, and large heat transfer enhancements can be obtained without any pressure penalty.

In the second tier, unsteady Reynolds averaged Navier Stokes simulations are conducted over a 2D numerical domain. Through the comparison of steady and averaged transient simulations, a wide range of excitation frequencies is explored. At low and moderate frequencies, with respect to the acoustic response of the domain, heat transfer and shear stresses are reduced. When exciting the domain at its resonance, a standing wave behavior is present, for which maximum heat transfer enhancement is observed. For larger frequencies, enhancement occurs near the leading edge of the plate, followed by a reduction close to the trailing edge. For all laminar conditions, there seems to be a positive correlation between the upstream boundary layer thickness and thermal streaming enhancement factor. For the turbulent case, the impact of the acoustic excitation is negligible for the investigated conditions.

Finally, the developed laminar model, which is an extension of Lin's method to traveling wave disturbances, provides a method to perform quick calculations of streaming effects in a laminar flow. Absent of any order of magnitude assumption, it allows resolution of traveling wave disturbances, previously ignored in literature. Comparison with the experiments reflect that the fluctuation amplitude and phase is resolved better than any previously considered reduced order model. Analyzing the nonlinear contribution of these fluctuations, it is shown that a particular combination of fluctuation parameters can yield either a reduction or enhancement in heat transfer through the streaming process.

To consider the cost of streaming, the acoustic power required for acoustic streaming can be calculated using the inlet velocity or pressure fluctuations. In the scope of the present research, the acoustic power required to excite the flow over flat plate is up to 2 W. If the flat plate is maintained at 900 K and the freestream flow is maintained at 300 K, the integrated heat transfer rate would be approximately 3 kW. A 10–15% enhancement, as shown in this paper, would then result in heat transfer rate increase by 300–450 W, which is considerably larger than the required acoustic power.

The potential application of this framework in a typical high Reynolds compressible flow environment would constitute the following steps. Due to the large number of parameters governing the aero-thermal streaming physics, the optimal heat transfer altering regions should be isolated by the laminar model through a response surface design. Then, the suggested conditions should be verified in the turbulent flow regime through 2D URANS simulations. As the Reynolds stresses are correlated with the mean flow quantities, the inherent turbulence models may provide inaccuracies. Therefore, the desired set of parameters should be verified with DNS to obtain quantitative high-fidelity results.

In conclusion, if streaming is implemented adequately to forced convection problems, the additional gradients at the solid–fluid interface introduces a possibility to enhance or reduce heat transfer in attached aero-thermal boundary layers. In the gas turbine community, this is relevant to augment heat transfer where pressure drop constraints exists or to shield surfaces from high temperatures present in external flows. For example, a direct application could be improving the heat exchange in turbine cooling passages and onboard heat exchangers, or reducing the heat transfer from the hot gas to the turbine blade surfaces. In practice, based on the optimal parameter space, the perturbations required for internal cooling channels can be introduced by a rotating porous disk that adds pulsations to the flow. Or alternatively, the existing pressure fluctuations due to rotor–stator interaction can readily be utilized to modulate the time-averaged heat transfer in both external turbine surfaces and internal cooling passages. Interestingly, this effect might already be inherently occurring in current turbine geometries, yet it has not been prior accounted for.

Acknowledgment

The present research effort was partially supported by Binational Science Foundation under grant 2016358. Furthermore, the authors would greatly appreciate the support of Uzi & Michal Halevy Grant for Innovative Applied Engineering and Henri Gutwirth Grant for Promotion of Excellence in Research.

Funding Data

- United States - Israel Binational Science Foundation (Grant No. 2016358; Funder ID: 10.13039/100006221).
- Uzi & Michal Halevy Grant for Innovative Applied Engineering and Henri Gutwirth Grant for Promotion of Excellence in Research.

Nomenclature

Symbol Description

A_f^+ = dimensionless forcing amplitude
C_p = specific heat capacity of fluid, (J/(kg.K))
f = frequency of oscillation, (Hz)
h = heat transfer coefficient, (W/(m^2.K))
k_f = thermal conductivity of fluid, (W/(m.K))
M_b = Mach number based on bulk velocity
Nu = Nusselt number
P_o = total pressure at the inlet, (kPa)
Pr = Prandtl number
Q = velocity of disturbance, (m/s)
Re = Reynolds number
T_o = isothermal flat plate temperature, (K)
T_∞ = free stream temperature, (K)
U = velocity fluctuations at free stream, (m/s)
U_b = bulk channel velocity, (m/s)
U_o = free stream velocity oscillations amplitude, (m/s)
U_∞ = free stream mean flow velocity, (m/s)
ν = kinematic viscosity, (m^2/s)
ΔP_o = total pressure fluctuations amplitude, (Pa)
η = nondimensionalized distance from wall; $= y/\sqrt{\nu/\omega}$
η_s = Stokes layer thickness; $\sqrt{\nu/\omega}$, (m)
ξ = nondimensional frequency parameter; $= \omega x/U_\infty$
ω = angular frequency of oscillation, (rad/s)

Abbreviations Description

DNS = direct numerical simulation
SEF = shear enhancement factor
TEF = thermal enhancement factor

References

[1] Kalinin, E. K., and Dreitser, G. A., 1998, "Heat Transfer Enhancement in Heat Exchangers," Adv. Heat Transfer, **31**, pp. 159–332.
[2] Lighthill, S. J., 1954, "The Response of Laminar Skin Friction and Heat Transfer to Fluctuations in the Stream Velocity," Proc. R. Soc. London. Ser. A. Math. Phys. Sci., **224**(1156), pp.1–23.
[3] Telionis, D. P., and Romaniuk, M. S., 1978, "Velocity and Temperature Streaming in Oscillating Boundary Layers," AIAA J., **16**(5), pp. 488–495.
[4] Stuart, J. T., 1966, "Double Boundary Layers in Oscillatory Viscous Flow," J. Fluid Mech., **24**(4), pp. 673–687.
[5] Lin, C. C., 1957, "Motion in the Boundary Layer With a Rapidly Oscillating External Flow," Ninth International Congress of Applied Mechanics, Brussels, Belgium, Sept. 5–13, p. 155.
[6] Patel, M. H., 1975, "On Laminar Boundary Layers in Oscillatory Flow," Proc. R. Soc. A Math. Phys. Eng. Sci., **347**(1648), pp. 99–123.
[7] Moschandreou, T., and Zamir, M., 1997, "Heat Transfer in a Tube With Pulsating Flow and Constant Heat Flux," Int. J. Heat Mass Transfer, **40**(10), pp. 2461–2466.
[8] Saavedra, J., Paniagua, G., and Lavagnoli, S., 2018, "On the Transient Response of the Turbulent Boundary Layer Inception in Compressible Flows," J. Fluid Mech., **850**, pp. 1117–1141.
[9] Scotti, A., and Piomelli, U., 2001, "Numerical Simulation of Pulsating Turbulent Channel Flow," Phys. Fluids, **13**(5), pp. 1367–1384.
[10] Costamagna, P., Vittori, G., and Blondeaux, P., 2003, "Coherent Structures in Oscillatory Boundary Layers," J. Fluid Mech., **474**, pp. 1–33.
[11] Wang, L., and Lu, X. Y., 2004, "An Investigation of Turbulent Oscillatory Heat Transfer in Channel Flows by Large Eddy Simulation," Int. J. Heat Mass Transfer, **47**(10–11), pp. 2161–2172.
[12] Jensen, B. L., Sumer, B. M., and Fredsøe, J., 1989, "Turbulent Oscillatory Boundary Layers at High Reynolds Numbers," J. Fluid Mech., **206**, pp. 265–297.
[13] Hino, M., Sawamoto, M., and Takasu, S., 1976, "Experiments on Transition to Turbulence in an Oscillatory Pipe Flow," J. Fluid Mech., **75**(2), pp. 193–207.
[14] Sleath, J. F. A., 1987, "Turbulent Oscillatory Flow Over Rough Beds," J. Fluid Mech., **182**(1), pp. 369–409.
[15] Hill, P. G., and Stenning, A. H., 1960, "Laminar Boundary Layers in Oscillatory Flow," J. Basic Eng., **82**(3), pp. 593–607.
[16] Nickerson, R. J., 1957, "The Effect of Free Stream Oscillations on the Laminar Boundary Layers on a Flat Plate," Ph.D. thesis, Massachusetts Institute of Technology, Cambridge, MA.
[17] Dec, J. E., Keller, J. O., and Arpaci, V. S., 1992, "Heat Transfer Enhancement in the Oscillating Turbulent Flow of a Pulse Combustor Tail Pipe," Int. J. Heat Mass Transfer, **35**(9), pp. 2311–2325.
[18] Keil, R. H., and Baird, M. H. I., 1971, "Enhancement of Heat Transfer by Flow Pulsation," Ind. Eng. Chem. Process Des. Dev., **10**(4), pp. 473–478.
[19] Kaiping, P., 1983, "Unsteady Forced Convective Heat Transfer From a Hot Film in Non-Reversing and Reversing Shear Flow," Int. J. Heat Mass Transfer, **26**(4), pp. 545–556.
[20] Niida, T., Yoshida, T., Yamashita, R., and Nakayama, S., 1974, "The Influence of Pulsation on Laminar Heat Transfer in Pipes," Chem. Eng., **38**(1), pp. 47–53.
[21] FUJITA, N., and TSUBOUCHI, T., 1982, "An Experimental Study of Unsteady Heat Transfer From a Flat Plate to an Oscillating Air Flow," Trans. Japan Soc. Mech. Eng. Series B, **48**(431), pp. 1330–1338.
[22] Jackson, T. W., and Purdy, K. R., 1965, "Resonant Pulsating Flow and Convective Heat Transfer," ASME J. Heat Transfer, **87**(4), pp. 507–512.
[23] Miller, J. A., 1969, "Heat Transfer in the Oscillating Turbulent Boundary Layer," ASME J. Eng. Power, **91**(4), pp. 239–244.
[24] Feiler, C. E., 1964, "Experimental Heat Transfer and Boundary Layer Behavior With 100-CPS Oscillations," NASA, Washington, DC, Report No. 2531.
[25] Martinelli, R. C., Boelter, L. M. K., Weinberg, E. B., and Yakahi, S., 1943, "Heat Transfer to a Fluid Flowing Periodically at Low Frequencies in a Vertical Tube," Trans. ASME, **65**, pp. 789–798.
[26] Barnett, D. O., and Vachon, R. I., 1970, "An Analysis of Convective Heat Transfer for Pulsating Flow in a Tube," Fourth International Heat Transfer Conference, Aug. 31–Sept. 5, Paris Versailles, France, pp. 1–11.
[27] Park, J. S., Taylor, M. F., and McEligot, D. M., 1982, "Heat Transfer to Pulsating Turbulent Gas Flow," Seventh International Heat Transfer Conference, Munich, West Germany, Sept. 8–10, pp. 105–110.
[28] Nagarajan, S., Lele, S. K., and Ferziger, J. H., 2003, "A Robust High-Order Compact Method for Large Eddy Simulation," J. Comput. Phys., **191**(2), pp. 392–419.
[29] Menter, F. R., 1994, "Two-Equation Eddy-Viscosity Turbulence Models for Engineering Applications," AIAA J., **32**(8), pp. 1598–1605.
[30] Celik, I. B., Ghia, U., and Roache, P. J., 2008, "Procedure for Estimation and Reporting of Uncertainty Due to Discretization in CFD Applications," ASME J. Fluids Eng, **130**(7), p. 078001.
[31] Schlichting, H., and Gersten, K., 2017, *Boundary- Layer Theory*, Springer-Verlag, New York.
[32] Agarwal, T., Julius, S., Leizeronok, B., and Cukurel, B., 2017, "Sound Excitation Effects on Forced Convection Heat Transfer," Active Flow Control: Techniques and Applications, VKI LS2017-04.
[33] Chan, T. F., 1984, "Stability Analysis of Finite Difference Schemes for the Advection-Diffusion Equation," SIAM J. Numer. Anal., **21**(2), pp. 272–284.
[34] Thomas, L., 1949, "Elliptic Problems in Linear Differential Equations Over a Network," Watson Scientific Computing Laboratory Report, Columbia University, New York.

[35] Coleman, G. N., Kim, J., and Moser, R. D., 1995, "A Numerical Study of Turbulent Supersonic Isothermal-Wall Channel Flow," J. Fluid Mech., **305**(1), p. 159.
[36] Evans, R. L., 1989, "Computation of Unsteady Laminar Boundary Layers Subject to Traveling-Wave Freestream Fluctuations," AIAA Journal, **27**(11), pp. 1644–1646.
[37] Spalart, P., 2000, "Strategies for Turbulence Modelling and Simulations," Int. J. Heat Fluid Flow, **21**(3), pp. 252–263.
[38] Yao, J., Chen, X., and Hussain, F., 2018, "Drag Control in Wall-Bounded Turbulent Flows Via Spanwise Opposed Wall-Jet Forcing," J. Fluid Mech., **852**, pp. 678–709.
[39] Rahbari, I., and Scalo, C., 2016, "Linear Stability Analysis of Compressible Channel Flow Over Porous Walls," *Whither Turbulence and Big Data in the 21st Century*?, Springer International Publishing, Cham, Switzerland, pp. 451–467.
[40] Clark, J. P., and Grover, E. A., 2007, "Assessing Convergence in Predictions of Periodic-Unsteady Flowfields," ASME J. Turbomach., **129**(4), p. 740.